

Maximum Flux Transition Paths of Conformational Change

Ruijun Zhao, Juanfang Shen, and Robert D. Skeel
Department of Computer Science, Purdue University
West Lafayette, IN 47907-2107

December 22, 2009

Abstract

Given two metastable states A and B of a biomolecular system, the problem is to calculate the likely paths of the transition from A to B . Such a calculation is more informative and more manageable if done for a reduced set of collective variables chosen so that paths cluster in collective variable space. The computational task becomes that of computing the “center” of such a cluster. A good way to define the center employs the concept of a committor, whose value at a point in collective variable space is the probability that a trajectory at that point will reach B before A . The committor “foliates” the transition region into a set of isocommittors. The maximum flux transition path is defined as a path that crosses each isocommittor at a point which (locally) has the highest crossing rate of distinct reactive trajectories. (This path is different from that of the MaxFlux method of Huo and Straub.) It is argued that such a path is nearer to an ideal path than others that have been proposed with the possible exception of the finite-temperature string method path. To make the calculation tractable, three approximations are introduced, yielding a path that is the solution of a nonsingular two-point boundary-value problem. For such a problem, one can construct a simple and robust algorithm. One such algorithm and its performance is discussed.

1 Summary

Considered here is the problem of computing transition paths of conformational change, given two different metastable states of a biomolecule. One motivation for this is to facilitate the accurate calculation of free energy differences. Another motivation is to determine the existence and structure of transition states and intermediate metastable states. The latter are possible targets for inhibitors of enhanced specificity in cases where a family of proteins have active sites with very similar structure. A good example of this situation is the Src tyrosine kinase family [39], which has long been implicated in the development of cancer. For this

system there are already computational results [11, 24, 38], supported by experiment [25], for the transition path from an active catalytic domain to an inactive catalytic domain.

Some approaches to this problem generate ensembles of trajectories based on the equations of motion. Notable examples are transition path sampling [2] and Markov state models [32]. Applying such methods to large proteins (without compromise) would appear to require exceptional computing capabilities, so here we pursue a more theoretical approach that avoids “direct numerical simulation.” Such approaches, like those in Refs. [13, 22, 27], seek to characterize one (or several isolated) “representative” reaction paths connecting two given metastable states, each path representing a bundle or cluster of trajectories. Here we adopt a well developed and tested theory, namely, transition path theory (TPT) [8, 20, 21, 33]. Additional references on computing transition paths are found in Ref. [26]. In general, it may also be of interest to calculate (i) the reaction rate for each bundle, or, at least, the relative rate for different bundles, and (ii) the potential of mean force. Here we consider only the calculation of the path itself.

In a nutshell, this article embraces a certain aspect of TPT and carries it to a logical conclusion, obtaining a formula, an implementation, and a proof of concept. The claim is that we can compute a path that is closer to the ideal than the minimum free energy path (MFEP) [20] and that, in a couple of respects, is better than the path of the finite-temperature string (FTS) method [29, 36], though inferior in another (important) respect. Additionally, the formula for the path is computationally more attractive than the formula that underlies either the path of the FTS method *or the MFEP*.

1.1 Outline and discussion

There are two distinct steps in getting a solution: The first is to define the problem without concern for the methods to be employed (other than taking into account the intrinsic difficulty of the problem). Defining a problem apart from a method gives a more concise definition. Also, by not guessing about what is feasible computationally, one may avoid unnecessary compromises. The second step is to construct a method and algorithm.

Given two metastable states A and B of a biomolecular system, the aim is to calculate the likely paths of the transition from A to B . Such a calculation is more informative and more manageable if done for a reduced set of *collective variables*, functions of the system configuration x ,

$$\zeta_1 = \xi_1(x), \zeta_2 = \xi_2(x), \dots, \zeta_\nu = \xi_\nu(x), \quad \text{abbreviated as } \zeta = \xi(x),$$

chosen so that paths cluster in collective variable space. The computational task becomes that of computing the “center” of such a cluster. A good way to define the center employs the concept of a committor, whose value at a point in collective variable space is the probability that a trajectory at that point will reach B before A . The committor “foliates” the transition region into a set of committor isosurfaces known as isocommittors. The maximum flux transition path (MFTP) is defined as a path that intersects each isocommittor at a point which (locally) has the highest crossing rate of distinct reactive trajectories. The MFTP is

not to be confused with MaxFlux method [1, 13]; it differs in several respects, in particular, the MFTP considers the flux of only those trajectories that are reactive (by using a result from TPT). A more detailed account of the problem definition is given in Section 2.

The minimum free energy path has been used for some time to represent reactive trajectories in collective variable space. Only fairly recently has its relationship to reactive trajectories been explained. The article [20] applies large deviation theory to show that the MFEP is the most probable path in the zero temperature limit of dynamics on a free energy surface defined at finite temperature. Hence, the MFEP is an inherently inconsistent construct and it is *useful only to the extent that it represents fully finite-temperature trajectories*. In fact, it does this fairly well on the simple tests reported here. Other fully finite-temperature constructs have been proposed: the finite-temperature string method in collective variable space (Sec. IV.B of Ref. [29]) and the swarm-of-trajectories string method [26], which constructs a Brownian dynamics model on the fly and constructs a path whose tangent is the most probable direction. How they differ from the MFTP is detailed in Section 2.

To make the calculation tractable, three approximations are introduced. To make the committor a more accessible quantity, the set of paths is approximated by a Brownian dynamics model, resulting in a boundary value problem in ν -dimensional space. Then the number of space dimensions is reduced to one by assuming most of the transition paths are contained in a tube, resulting in a two-point boundary-value problem with 2ν unknowns. A third approximation reduces this to ν unknowns, whose solution is a *maximum flux transition path*. The resulting equations involve a free energy gradient term and an explicitly temperature-dependent curvature term. Specifically, the maximum flux transition path $\zeta = Z(s)$, $0 \leq s \leq 1$, is defined by the condition that

$$-\beta \nabla F(Z) + \frac{(D(Z)^{-1} Z_s)_s}{Z_s^\top D(Z)^{-1} Z_s} \parallel D(Z)^{-1} Z_s,$$

holds for $\zeta = Z(s)$ where β is the inverse temperature, $F(\zeta)$ is the free energy profile, $D(\zeta)$ is a proto-diffusion tensor depending on masses and ξ , and the subscript s denotes differentiation (d/ds). In the high temperature limit, the path becomes a straight line. In the low temperature limit, the path becomes an MFEP. At zero temperature the path will have cusps at some intermediate local minima, which presents difficulties if free energy profiles or relative reaction rates are to be determined. This formula is a key result of this article. Details are given in Section 3.

The temperature-dependent curvature term not only provides a finite temperature correction to the MFEP, but it yields a nonsingular second order ordinary differential equation, amenable to standard techniques—except for the need to do computationally intensive sampling to evaluate terms in the differential equation. An existing set of algorithms for the MFEP [6, 20] applies equally well to the MFTP. The equation is discretized using upwinded differencing and solved using the semi-implicit simplified string method [35]. (A notable alternative is the nudged elastic band method, introduced in Ref. [14].) Algorithmic details are provided in Section 4.

Section 5 compares the MFTP to the MFEP on numerical examples. First, an artificial problem in full configuration space is solved to demonstrate the effect of the curvature term

of the MFTP. (A problem in full configuration space is equivalent to a problem in collective variable space with perfect sampling.) In particular, the necessity of using an adaptive mesh for the MFEP is demonstrated. Then alanine dipeptide in vacuum is solved using the ϕ , ψ dihedrals as collective variables. For the transition path from $C_{7\text{ax}}$ to $C_{7\text{eq}}$ as in Ref. [20], the computational cost for calculating the MFTP and the MFEP is almost same. However, for a transition path from $C_{7\text{eq}}$ to $C'_{7\text{eq}}$ through $C_{7\text{ax}}$ shown in Ref. [29], the MFEP has a cusp at $C_{7\text{ax}}$ and the computational cost for finding such a cusp is expensive. On the other hand, the MFTP smooths out the cusp and the computational cost is reduced.

An open source implementation of the MFTP method is available [40] as a relatively simple set of Python modules with examples using pure Python, CHARMM [4], and NAMD [28].

1.2 Conclusions

For alanine dipeptide, the MFEP, MFTP, and FTS method paths are quite similar. On a contrived problem with a rough energy landscape, e.g., Figure 2 in Ref. [36], the FTS method path gives a much better result. On a different contrived problem given in Section 5.1, the MFTP gives a much better result. Contrived examples are relevant because computational techniques are sometimes applied in extreme situations for which they may not have been designed. In terms of quality, the MFTP ranks higher than the MFEP but lower than the FTS method path (because the latter addresses the more serious difficulty of multiple local minima).

The minimum free energy path (and that of the FTS method) can have cusps at some intermediate metastable states, which makes it unsuitable for defining an isocommittor, unsuitable for defining a reaction coordinate, and harder to compute. Computational difficulties include the need for an adaptive mesh and a greater number of iterations until convergence.

2 What is the problem?

We begin by defining an ensemble of transition paths from A to B : For simplicity, assume the molecular system obeys Newtonian dynamics with potential energy function $U(x)$ and a diagonal matrix M of atomic masses. Positions x and momenta p satisfy $x = X(t)$, $p = P(t)$ where $(d/dt)X(t) = M^{-1}P(t)$ and $(d/dt)P(t) = -\nabla U(X(t))$. Initial values are drawn from a Boltzmann-Gibbs distribution $\rho(x, p)$: positions x from probability density $const e^{-\beta U(x)}$ and momenta p from a Maxwell distribution. Imagine an extremely long trajectory. The trajectory enters and leaves A and B many times yielding a huge set of reactive paths from A to B . (A reactive path is a piece of the trajectory outside of A and B that comes from A and goes to B .)

Generating an ensemble of trajectories is extremely demanding computationally. And, even if this were possible, what would the user do with all the data? By answering such a question, we might well avoid the task of computing trajectories. It is likely that one would cluster the trajectories to produce a concise description. Therefore, one might instead directly determine such a concise description. Specifically, if the paths cluster into one or

several distinct isolated bundles/tubes/channels/pathways, one might compute a “representative path” for each cluster. This idea is developed in the paragraphs that follow.

However, transition paths might not cluster adequately—in full configuration space. Assume, though, there is a smaller set of collective variables, $\zeta = \xi(x)$, such that in ζ -space, paths cluster into one or several distinct isolated channels connecting two separated subsets A_ξ and B_ξ of collective variable space. Otherwise, there is little of interest to compute. A typical example of collective variables is ϕ/ψ angles along a peptide backbone. Once the collective variables are specified, the problem is to calculate a path in collective variable space, $\zeta = Z(s)$, $0 \leq s \leq 1$, connecting A_ξ to B_ξ where the transition paths are concentrated. Along with a parameterization of the path in collective variable coordinates, would be a realization of it in cartesian coordinates, so once the path is generated, structures can be studied as well. A drawback of this approach is the need to identify an appropriate set of collective variables. Indeed, defining suitable collective variables is an important research problem [17].

We want a minimal set of collective variables subject to two conditions: First, the coordinates ζ must suffice to describe states A_ξ , B_ξ in ζ -space corresponding to A , B . Second, coordinates ζ must also be rich enough to “express the mechanism of conformational change” along the transition path. To make the second condition more precise, we introduce the notion of “quasi-committor.”

To measure the progress of a transition, there is a natural reaction coordinate, known as the *committor*. This concept of a commitment probability was introduced by Onsager [23], and the abbreviated term “committor” was introduced in Ref. [3] (p. 9236), which they defined as follows: For each point x in configuration space, consider a trajectory starting with $X(0) = x$ and velocities drawn at random from a Maxwell distribution, and define the committor $q(x)$ to be the probability of reaching B before A . Since it is the coordinates of the collective variables that are of interest, it is natural also to define a *quasi-committor*: For each point ζ , consider a trajectory starting with random initial values *conditioned on* $\xi(x) = \zeta$ and define the quasi-committor $\hat{q}(\zeta)$ to be the probability of reaching B_ξ before A_ξ :

$$\hat{q}(\zeta) = \Pr(\xi(X(t)) \text{ reaches } B_\xi \text{ before } A_\xi \mid \xi(X(0)) = \zeta).$$

We could say that the variables $\zeta = \xi(x)$ are rich enough to express the mechanism of conformational change if the quasi-committor $\hat{q}(\zeta)$ has no local minima or maxima outside of A_ξ and B_ξ (except for regions of negligible probability). Otherwise, there is some unexpressed degree of freedom important to the transition. As an example, suppose that virtually all trajectories stay within a narrow tube having a geometry in full configuration space illustrated by 1. Suppose that the free energy profile *as a function of arc length* along the transition tube is much higher in the backward section than it is in the two forward sections. Then most of the increase in the quasi-committor as a function of arc length occurs in the middle section of the tube. Consequently, the variation in the quasi-committor, as a function of the ill-chosen collective variable ζ corresponding to the horizontal axis, will be dominated by this middle section of the tube. This results in a graph of $\hat{q}(\zeta)$ that increases at the beginning and end of its range but decreases in the middle part. In addition to $\hat{q}(\zeta)$

having no local extrema, it is desirable that $\hat{q}(\xi(x)) \approx q(x)$. The quality of the collective variables can be checked in principle by calculating quasi-committor values $\hat{q}(\zeta)$ at points along the path from dynamics trajectories.

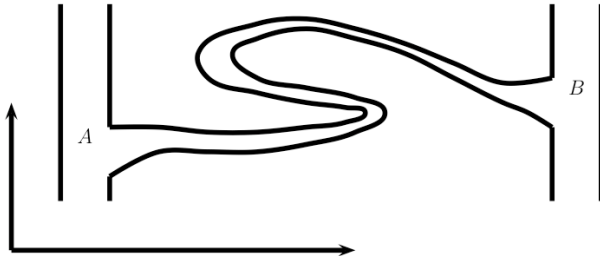


Figure 1: A schematic illustration of a poor choice of collective variables. The horizontal axis is collective variables, and the vertical axis is unrepresented degrees of freedom. The collective variables fail to indicate the progress of the reaction.

Two approaches have been proposed for defining the center of a cluster of paths in ζ -space:

- (i) a most probable path, e.g., a swarm-of-trajectories string method [26, 34] path, and
- (ii) a path that intersects each isosurface of the quasi-committor at a center of the collection of points where reactive trajectories cross that isosurface, e.g., a finite temperature string method [29] path and a *maximum flux transition path*.

An MFEP is a limiting case of both approaches. (The MFEP is obtained from these various approaches by letting $\beta \rightarrow \infty$ in the path formula but not in the definition of the free energy profile.) Defining the objective is a compromise between (i) best capturing the object of interest and (ii) simplicity.

One problem with seeking the most probable path is that it is unclear how to assign relative probabilities to paths. More importantly, the most probable path tends to be a path of minimum energy, and it is not clear—a priori—that this is a “representative” path. For Hamiltonian dynamics, it would seem that the probability that we attach to a path would be proportional to $\exp(-\beta E)$ where E is the energy. Hence, the most probable path is the one with just enough energy to surmount the potential energy barriers. For stochastic dynamics, the explanation of how to assign probability to paths is quite complicated—if paths of different durations are being compared. An explanation for Brownian dynamics is possible using Freidlin-Wentzell theory and the assumption of vanishingly small noise (see Appendix A of Ref. [20]). It is reassuring though that the results of Freidlin-Wentzell theory agree with those of TPT in the zero-temperature limit (for $F(\zeta)$ held fixed).

For defining a path in terms of an intersecting point on each isosurface of a quasi-committor, one needs

- (i) a definition for the distribution of crossing points of reactive trajectories through a quasi-committor isosurface and

- (ii) a definition of centrality, e.g., mode, median, or mean.

We consider each of these in turn.

The finite-temperature string method defines the distribution of crossing points of reactive trajectories in a way that includes recrossings. A subsequent article [21] illustrates the dramatic distortions that arise by including recrossings, and it emphasizes crossings of a surface by distinct reactive trajectories instead of all crossings by reactive trajectories. They define such a distribution in terms of the net crossings of reactive trajectories across each infinitesimal piece of a surface. It is not obvious, however, that this necessarily gives nonnegative values on the isosurface of a quasi-committor, so, instead, we use the density of last crossings by reactive trajectories, called *last hitting points* in Ref. [8]. For the Brownian dynamics approximation developed in the next section, these two measures are identical.

Consider now the question of defining the center. Let $j(\zeta)$ denote the density associated with a definition for the distribution of crossing points of reactive trajectories through a quasi-committor isosurface. One choice for the center is the point of highest probability. In other words, seek the path $\zeta = Z(s)$, $0 \leq s \leq 1$, each of whose points $Z(s)$ is a local maximum of the density $j(\zeta)$ on the quasi-committor isosurface Σ passing through $Z(s)$. This is what we use for the MFTP. Another choice, associated with the *finite-temperature string method*, is to construct the path from the mean value ζ' on each quasi-committor isosurface Σ : the point ζ' that minimizes $\int_{\Sigma} |\zeta' - \zeta|^2 j(\zeta) d\zeta$. Although this notion is a superior measure of centrality, it is more complicated to explain. In practice, methods for finding a maximum are designed only to find a local maximum, which is what we do for the MFTP. This is satisfactory if there is a choice of collective variables that produces a free energy landscape free of roughness at the scale of the thermal energy [36]. In any case, the equations defining a center-of-density path are intrinsically more expensive computationally to solve than those for the MFTP, because they require averaging on quasi-committor isosurfaces $\hat{q}(\zeta) = \text{constant}$ (in addition to conditional averages on collective variable isosurfaces $\xi(x) = \zeta$ in full configuration space) rather than merely determining a (local) maximum.

3 A method

As stated previously, computing $\hat{q}(\zeta)$ is not feasible. Consequently, we derive a method, which employs three uncontrolled approximations—a controlled approximation being one that can be made arbitrarily accurate with sufficient computational effort. Subsection 3.1 approximates paths in collective variable space by those of Brownian dynamics; Subsection 3.5 assumes most paths lie in a tube where isocommittors are planar; and Subsection 3.6 assumes that on average the trajectories are parallel to the path. The basic ingredients of much of this development are present in the literature but scattered among several articles. Here they are combined to produce equations from which we derive the MFTP.

3.1 Brownian dynamics approximation of collective variable paths

The probability density function (p.d.f.) for $\xi(x)$ is

$$\rho_\xi(\zeta) = \langle \delta(\xi(x) - \zeta) \rangle = \iint \delta(\xi(x) - \zeta) \rho(x, p) dx dp$$

where $\delta(\zeta) = \delta(\zeta_1)\delta(\zeta_2)\cdots\delta(\zeta_\nu)$. Let $\langle \cdot \rangle_\zeta$ be the expectation for the conditional density $\rho(x, p | \xi(x) = \zeta)$:

$$\langle O(x) \rangle_\zeta = \frac{\langle \delta(\xi(x) - \zeta) O(x) \rangle}{\langle \delta(\xi(x) - \zeta) \rangle}.$$

In Appendix A is an adaptation of an argument from Ref. [20] (Sec. III, A and B) suggesting that as an approximation to $\hat{q}(\zeta)$, we should seek a function $q(\zeta)$ that minimizes a certain functional $I(q)$ that can be expressed in terms of collective variables ζ . Define the free energy $F(\zeta)$ for coordinates $\zeta = \xi(x)$ by

$$\text{const}_\xi e^{-\beta F(\zeta)} = \rho_\xi(\zeta) = \langle \delta(\xi(x) - \zeta) \rangle. \quad (1)$$

Also define a proto-diffusion tensor D by

$$D(\zeta) = \frac{1}{2} \beta^{-1} \langle \xi_x(x) M^{-1} \xi_x(x)^\top \rangle_\zeta.$$

(There is freedom in the scaling of D . We use this freedom to make Eq. (4) agree with an alternative derivation of the Brownian dynamics, in which one assumes instantaneous relaxation of the degrees of freedom not represented by the collective variables. The tensor $D(\zeta)$ fails to be a diffusion tensor because it is missing a time scale factor.) The functional is then

$$I(q) = \text{const}_\xi \int e^{-\beta F(\zeta)} \nabla q(\zeta)^\top D(\zeta) \nabla q(\zeta) d\zeta \quad (2)$$

where the integral is over the transition region outside of A_ξ and B_ξ subject to $q(\zeta) = 0$ on the boundary of A_ξ and $q(\zeta) = 1$ on the boundary of B_ξ .

The corresponding Euler-Lagrange equation for $q(\zeta)$ is the Smoluchowski (backward Kolmogorov) equation:

$$-\nabla \cdot e^{-\beta F(\zeta)} D(\zeta) \nabla q(\zeta) = 0, \quad (3)$$

subject to $q(\zeta) = 0$ on the boundary of A_ξ and $q(\zeta) = 1$ on the boundary of B_ξ .

The function q that satisfies the Smoluchowski equation subject to the given boundary conditions can be shown to be the exact committor function for paths $\zeta = \zeta(\tau)$ in collective variable space generated by the Brownian dynamics

$$\frac{d}{d\tau} \zeta = -\beta D(\zeta) \nabla F(\zeta) + (\nabla \cdot D(\zeta))^\top + \sqrt{2} D_{1/2}(\zeta) \eta(\tau) \quad (4)$$

where $D_{1/2} D_{1/2}^\top = D$ and $\eta(\tau)$ is a collection of standard white noise processes. The fact that τ is an artificial time does not affect the committor. In principle, the assumption $q(\zeta) \approx \hat{q}(\zeta)$

can be checked a posteriori by comparing committor values of the Brownian dynamics to the quasi-committor values of actual dynamics.

Reference [20] (Sec. III.C) appears to suggest that the Smoluchowski equation uniquely specifies dynamics except for scaling of time: If the Smoluchowski equation (3) is satisfied by committors $q(\zeta)$ for arbitrary sets A'_ξ and B'_ξ in collective variable space, then trajectories whose committor functions satisfy Eq. (3) must have paths that are those of the Brownian dynamics. Hence, paths in collective variable space can be generated with the proper probabilities from the system of stochastic differential equations.

3.2 Last hitting-point distribution

Appendix B considers the rate at which reactive trajectories cross an arbitrary surface Σ that separates collective variable space into two parts, one containing A_ξ and the other containing B_ξ . The result given there is that the rate of the *last* crossing of Σ by reactive trajectories is given by the integral

$$\int_{\Sigma} J(\zeta) \cdot \hat{n}(\zeta) dS_{\zeta},$$

where $\hat{n}(\zeta)$ points to the side containing B_ξ , and

$$J(\zeta) = \rho_\xi(\zeta) D(\zeta) \nabla q(\zeta)$$

is the last hitting-point flux. The choice of the last hitting point to represent the point where a reactive trajectory crosses an isocommittor is somewhat arbitrary. Therefore, it is gratifying to know that the expression for $J(\zeta)$ also gives the net flux and the first hitting-point flux of reactive trajectories.

The normal to an isocommittor is given by $\hat{n}(\zeta) = \nabla q(\zeta) / |\nabla q(\zeta)|$, so the distribution of last hitting points on an isocommittor is proportional to

$$j(\zeta) = \rho_\xi(\zeta) \nabla q(\zeta)^\top D(\zeta) \nabla q(\zeta) / |\nabla q(\zeta)|.$$

3.3 Defining the path

For computation it is convenient to label the isocommittors with the path parameter s . In particular, denote by $\Sigma(s)$, $0 \leq s \leq 1$, the isocommittor passing through $\zeta = Z(s)$. Write $\bar{q}(s) = q(Z(s))$ and define $\sigma(\zeta)$ implicitly by

$$q(\zeta) = \bar{q}(\sigma(\zeta)). \tag{5}$$

In this way the committor $q(\zeta)$ is decomposed into two independent parts: one part $\sigma(\zeta)$ specifies the isocommittor label and the other part $\bar{q}(s)$ calibrates the isocommittors. On an isocommittor $\Sigma(s)$, the gradient $\nabla q(\zeta) = \bar{q}_s(\sigma(\zeta)) \nabla \sigma(\zeta)$, so the normal flux is

$$j(\zeta) = \bar{q}_s(\sigma(\zeta)) \rho_\xi(\zeta) \nabla \sigma(\zeta)^\top D(\zeta) \nabla \sigma(\zeta) / |\nabla \sigma(\zeta)| \tag{6}$$

(recalling that the subscript s denotes differentiation d/ds). Note that \bar{q}_s contributes only a scale factor to $j(\zeta)$, so the center of intensity on $\Sigma(s)$ does not depend on \bar{q}_s .

Each point $Z(s)$ on the desired path maximizes the last hitting-point flux $j(\zeta)$ on the isocommittor $q(\zeta) = q(Z(s))$. Hence, $\nabla j(Z(s)) \parallel \nabla q(Z(s))$. To keep the derivation independent of the calibration $\bar{q}(s)$, introduce a vector $n(s)$, not necessarily normalized, such that $n(s) \parallel \nabla q(Z(s))$. Hence,

$$\nabla j(Z(s)) \parallel n(s). \quad (7)$$

3.4 The localized tube assumption

Assume there exists a tube connecting A_ξ to B_ξ such that (i) on each isocommittor, regions of high $j(\zeta)$ are concentrated in the tube, (ii) each isocommittor is nearly planar in the tube, and (iii) $D(\zeta)$ is nearly constant on each isocommittor within the tube. This scenario is illustrated in 2 below.

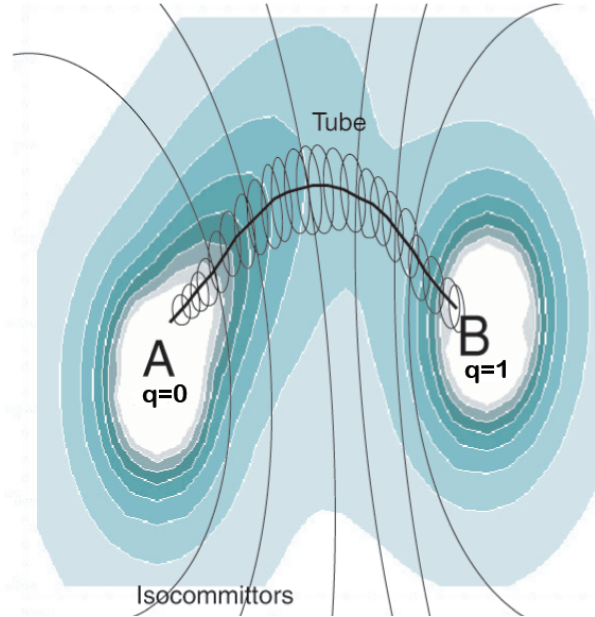


Figure 2: Shading indicates contours of free energy, thin curves denote isocommittors, ellipses enclose concentrations of crossing points from reactive trajectories, and the thick curve is the center.

Exploit the localized tube assumption by approximating the isocommittor through $Z(s)$ as a plane $\Pi(s)$ with normal $n(s)$. Hence, the isocommittor surface $\Sigma(s) : \sigma(\zeta) = s$ has the simple description of a hyperplane,

$$\Pi(s) : n(s) \cdot (\zeta - Z(s)) = 0. \quad (8)$$

Also, approximate $D(\zeta)$ by $\bar{D}(\sigma(\zeta))$ where $\bar{D}(s) \stackrel{\text{def}}{=} D(Z(s))$. These approximations (see Ref. [33] (Sec. 6.6.1)) are sufficient to define a practical method (see Ref. [7] (Sec. 12)). The unknown direction vector $n(s)$ is to be chosen to minimize the integral $I(q)$ of Eq. (2) restricted to some tube. For simplicity the boundary points $Z(0)$ and $Z(1)$ can be moved to points in A_ξ and B_ξ that locally minimize $F(\zeta)$. In this way the problem of solving for a committor of many variables is reduced to that of a one-dimensional calculation along the length of the tube.

It remains to derive the condition that determines $Z(s)$. This is done in Appendix C, where it is shown that the condition is

$$-\beta \nabla F(Z) + \frac{n_s}{n^\top Z_s} \parallel n.$$

3.5 The maximum flux transition path

Although the localized tube assumption is sufficient for defining a practical method, the method would not be simple, so we make an additional simplifying assumption: Assume the flux $J(\zeta)$ points in the direction of the path so that $J(Z(s)) \parallel Z_s(s)$ or $D(Z(s))\nabla q(Z(s)) \parallel Z_s(s)$, whence

$$n(s) \parallel D(Z(s))^{-1} Z_s(s).$$

The result is a *maximum flux transition path*

$$-\beta \nabla F(Z) + \frac{(D(Z)^{-1} Z_s)_s}{Z_s^\top D(Z)^{-1} Z_s} \parallel D(Z)^{-1} Z_s. \quad (9)$$

(The simplifying assumption is justified, for example, if the probability is strongly peaked around the path, resulting in most of the probability contained in a narrow tube with a flux $J(\zeta)$ pointing in the direction of the tube and the path.) This assumption is also made for the FTS method, see Eq. (14) of Ref. [29] and Sec. II.A. of Ref. [36]. Geometrically, this condition means that instead of having the free energy gradient vanish orthogonal to the path, it is balanced by a ‘‘centripetal’’ force, which reduces curvature and avoids cusps.

To express condition (9) as an equation, write it as $-\beta(Z_s^\top D^{-1} Z_s) D \nabla F + D(D^{-1} Z_s)_s = \lambda Z_s$ where λ is a scalar and premultiply by Z_s^\top to obtain an expression for λ . After eliminating λ , the equation becomes

$$(I - \Pi) D(D^{-1} Z_s)_s = (I - \Pi) \beta (Z_s^\top D^{-1} Z_s) D \nabla F \quad (10)$$

where the projector

$$\Pi = Z_s Z_s^\top / (Z_s^\top Z_s).$$

Note that, if D is constant, the limit $\beta \rightarrow 0$ for Eq. (10) gives a geodesic $Z_{ss} = 0$, which is the desired result.

In the two-dimensional case with $D = I$, the Euclidean length of $(I - \Pi) D(D^{-1} Z_s)_s / (Z_s^\top D^{-1} Z_s)$ is exactly equal to the curvature, which is defined to be the reciprocal of the radius of curvature. To see this, note that this is true if we parameterize with (actual) arc length and

note also that the curvature term is independent of parameterization (which can be checked analytically).

If we normalize the parameterization using $(Z_s^\top Z_s)_s = 0$, this implies $Z_s^\top Z_{ss} = 0$ and $\Pi Z_{ss} = 0$. Adding this last equation to Eq. (10) gives a *nonsingular* second order ordinary differential equation for $Z(s)$:

$$Z_{ss} = (I - \Pi) (\beta(Z_s^\top D^{-1} Z_s) D \nabla F + D_s D^{-1} Z_s).$$

Values obtained from constructing the path can be used to calculate the free energy $F(Z(s))$ along the path,

$$F(Z(s)) - F(Z(0)) = \int_0^s \nabla F(Z(s'))^\top Z_s(s') ds'.$$

However, $F(Z(s))$ is not a potential of mean force for the transition.

3.6 The minimum free energy path

The simplifying assumption of the preceding subsection, which is used to derive the MFTP, is valid in the limit $\beta \rightarrow \infty$ in the Brownian dynamics approximation; see Ref. [33] (Sec. 6.6) and Ref. [20] (App. A). A more systematic derivation might therefore neglect the curvature term. The result would be a *minimum free energy path*

$$Z_s \parallel -\beta D(Z) \nabla F(Z).$$

Each point $\zeta = Z(s)$ on the MFEP is a local minimum of $F(\zeta)$ in the hyper-plane orthogonal to $D(Z(s))^{-1} Z_s(s)$.

One difference from an MFTP is that an MFEP can have a cusp at an intermediate local minimum. If the path passes sufficiently close to a local minimum $\zeta = \zeta_0$ of $F(\zeta)$, then for a short section of the path, $\zeta = Z(s)$, $a \leq s \leq b$, a quadratic approximation to $F(\zeta)$ is accurate. Assume $D = \text{constant}$ and $F(\zeta) = \frac{1}{2}(\zeta - \zeta_0)^\top A(\zeta - \zeta_0) + \text{constant}$, where A is symmetric positive definite. The MFEP is then defined by $Z_s \parallel -\beta D A (Z - \zeta_0)$. Perform a change of variables, $Y = \beta^{-1/2} Q^\top D_{1/2}^{-1} (Z - \zeta_0)$ where $Q \Lambda Q^\top$ is a diagonalization of $D_{1/2}^\top A D_{1/2}$. The MFEP for $Y(s)$ is hence given by $Y_s \parallel -\Lambda Y$. For simplicity, suppose that $Y = [x, y]^\top$, that $x(a) < 0 < x(b)$, and that $\Lambda = \text{diag}(\lambda, \mu)$ with $\lambda > \mu$. The path is hence defined by $y_s/(\mu y) = x_s/(\lambda x)$, which can be integrated to yield the path

$$y = \begin{cases} (x/x(a))^{\mu/\lambda} y(a), & x(a) \leq x \leq 0, \\ (x/x(b))^{\mu/\lambda} y(b), & 0 \leq x \leq x(b), \end{cases}$$

which has a cusp at $x = 0$.

The FTS method path is also likely to suffer from the presence of cusps, because for a harmonic potential, the average position is the same as the most probable position.

The presence of cusps undermines the localized tube assumption. In particular, the assumption of isocommitters being approximately planar breaks down at a cusp. This poses a difficulty when computing transition rates, which depends on existence of isocommitters. Additionally, cusps complicate the numerical approximation of paths.

4 An algorithm

An algorithm for calculating a transition path employs a progression of four controlled approximations: discretization of the path $\zeta = Z(s)$ and the equations that define it; a finite number of iterations for the solution of nonlinear discrete equations; use of restraints for constrained sampling; and finite sampling.

4.1 Discretization

The path $Z(s)$, $0 \leq s \leq 1$, is approximated as a piecewise polynomial with break points $0 = s_0 < s_1 < \dots < s_J = 1$. Here we choose a uniform mesh $s = 0, \Delta s, \dots, 1$ and obtain the path by piecewise linear interpolation. Thus the problem is reduced to determining *unknown* nodal values $Z_j \approx Z(s_j)$, $j = 0, 1, \dots, J$, each representing a replica of the system in a different configuration.

It is convenient for computation to use for the path parameter s the arc length along the path divided by the total length of the path. In such a case, $|Z_s(s)|$ is constant. The arc length normalization becomes

$$|Z_{j+1} - Z_j|/\Delta s = |Z_j - Z_{j-1}|/\Delta s, \quad j = 1, 2, \dots, J - 1.$$

Condition (9) is written as

$$-\beta D \nabla F + \frac{1}{c} Z_{ss} - \frac{1}{c} D_s D^{-1} Z_s \parallel Z_s$$

where $c = Z_s^\top D^{-1} Z_s$.

This is discretized by the finite difference scheme

$$(Z_s)_j \parallel g_j, \quad \text{where } g_j \stackrel{\text{def}}{=} -\beta D_j (\nabla F)_j + \frac{1}{c_j} \frac{Z_{j+1} - 2Z_j + Z_{j-1}}{\Delta s^2} - \frac{1}{c_j} (D_s D^{-1} Z_s)_j$$

and where

$$c_j = \frac{1}{2} \Delta s^{-2} (\Delta_- Z_j^\top D_j^{-1} \Delta_- Z_j + \Delta_+ Z_j^\top D_j^{-1} \Delta_+ Z_j), \quad (11)$$

$$(D_s D^{-1} Z_s)_j = \frac{1}{2} \Delta s^{-2} (\Delta_- D_j D_j^{-1} \Delta_- Z_j + \Delta_+ D_j D_j^{-1} \Delta_+ Z_j), \quad (12)$$

with

$$\Delta_\pm D_j = \mp (D_j - D_{j\pm 1}), \quad \text{and } \Delta_\pm Z_j = \mp (Z_j - Z_{j\pm 1}).$$

We choose upwinded differencing for $(Z_s)_j$ based on the direction of the modified mean force g_j :

$$(Z_s)_j = \begin{cases} (Z_j - Z_{j-1})/\Delta s & \text{if } g_j^\top (Z_j - Z_{j-1}) > 0, \\ (Z_{j+1} - Z_j)/\Delta s & \text{if } g_j^\top (Z_j - Z_{j+1}) > 0. \end{cases} \quad (13)$$

In the unlikely event that both conditions are satisfied, the choice is dictated by the arc length normalization step of the simplified string method to be discussed next.

For the MFEP, cusps can occur at some intermediate local minima, requiring an adaptive mesh to resolve.

4.2 Solution of nonlinear discrete equations

A second component of the algorithm is an iterative method for achieving rapid local convergence given a plausible initial guess.

Because of its simplicity and demonstrated effectiveness, we adopt the semi-implicit simplified string method used in Ref. [35] (Eq. (11)). To determine a path, begin with an initial guess and generate successive improvements by alternating between moving the points of the curve Z_j in the direction g_j given by condition (9) and reparameterizing.

The first step of each iteration is to solve the following equations for the Z_j^* :

$$\begin{aligned} \frac{Z_j^* - Z_j}{\tau^2} &= \frac{1}{c_j} \frac{Z_{j+1}^* - 2Z_j^* + Z_{j-1}^*}{\Delta s^2} - \frac{1}{c_j} (D_s D^{-1} Z_s)_j - \beta D_j (\nabla F)_j, \quad j = 1, 2, \dots, J-1, \\ \frac{Z_j^* - Z_j}{\tau^2} &= -\beta D_j (\nabla F)_j, \quad j = 0, J, \end{aligned}$$

where c_j and $(D_s D^{-1} Z_s)_j$ are given in Eqs. (11) and (12). (The extra factor τ provides the time scale factor missing from D .)

Then the normalization adjustment is to choose the $\{Z_j\}$ to be equidistant along the resulting curve:

$$\begin{aligned} s_0^* &= 0, s_j^* = s_{j-1}^* + |Z_j^* - Z_{j-1}^*|, \\ Z^*(s) &= \text{piecewise linear interpolation of } \{(s_j^*/s_j^*, Z_j^*)\}, \quad 0 \leq s \leq 1, \\ Z_j^{\text{new}} &= Z^*(j/J). \end{aligned}$$

It can be shown that if the semi-implicit simplified string method converges, the resulting points Z_j satisfy a nonstandard discretization of the differential equation containing τ as a parameter. In the limit $\tau \rightarrow 0$, the discretization becomes upwinded differencing.

For large systems, targeted molecular dynamics [31] has been used to get an initial path [11, 12]. Another potentially promising but quite different approach is rigidity analysis [16].

4.3 Conditional averages

Evaluation of ∇F and D at break points involves sampling on hyper-surfaces $\{x : \xi(x) = Z_j\}$ of configuration space.

For calculating such conditional expectations, the Dirac delta function $\delta(s)$ can be approximated by the p.d.f. of a Gaussian $\delta_\varepsilon(s) = (2\pi\varepsilon^2)^{-1/2} \exp(-s^2/(2\varepsilon^2))$. Note

$$\delta_\varepsilon(\xi(x) - \zeta) e^{-\beta U(x)} = (2\pi\varepsilon^2)^{-\nu/2} e^{-\beta U(x; \zeta)}$$

where

$$U(x; \zeta) = U(x) + \sum_{i=1}^{\nu} u_i(x, \zeta_i), \quad \text{and } u_i(x, \zeta_i) = \frac{1}{2\beta\varepsilon^2} (\xi_i(x) - \zeta_i)^2. \quad (14)$$

Then, $\langle O(x) \rangle_\zeta = \langle O(x) \delta_\varepsilon(\xi(x) - \zeta) \rangle / \langle \delta_\varepsilon(\xi(x) - \zeta) \rangle$ is nothing but an average using $U(x; \zeta)$. The effect is that of using restraining potentials instead of constraints. These restraints should be as strong as possible without restricting the step size used in the sampling. From $\text{const}_\xi \exp(-\beta F(\zeta)) = \langle \delta_\varepsilon(\xi(x) - \zeta) \rangle$, we have

$$\nabla F(\zeta) = -\frac{1}{\beta \varepsilon^2} \langle \xi(x) - \zeta \rangle_\zeta.$$

4.4 Sampling

We would like to estimate the statistical error of Z_j^* . Ideally, we want the standard deviation of the estimate smaller than some given tolerance. The major contribution to the sampling error of Z_j^* comes from that of $(\nabla F)_j$, because of the cancelation and subsequent multiplication by ε^{-2} . Thus, we neglect the statistical error of D_j in estimating the error of g_j . So then, the statistical error of Z_j^* comes from the sample average of $\Delta_j = \beta D_j (\nabla F)_j^n$, $n = 1, 2, \dots, N$, where N is the sample size. The statistical error is defined by $(\max_{0 \leq j \leq J} \text{error bar of } \Delta_j) \tau^2$, where an error bar is an estimate of 1 standard deviation. Such an estimate can be obtained using block averaging as in Ref. [10] (Appendix D.3). In general, 32 blocks is a reasonable choice.

At each iteration, the configuration x from the previous iteration could be used to start the equilibration of the molecular dynamics. Thus, it is necessary that values of x be stored such that $\xi(x) = Z_j$, $j = 0, 1, \dots, J$. It is reasonable to expect less equilibration time is needed in later iterations as the path converges.

5 Numerical tests

5.1 An artificial problem

As an example to illustrate our method, consider a problem finding the MFTP and MFEP for the potential energy function

$$\begin{aligned} U(x, y) = & -4 \exp(-4x^2 - (y - 2.75)^2) - 5 \exp(-(x - 1)^2 - (y - 0.15)^2) \\ & - 5 \exp(-(x + 1)^2 - y^2) + 8 \exp(-x^2 - (y + 0.5)^2) + 0.001(x^4 + y^4) \end{aligned}$$

where the energy unit is kcal/mol and the mass matrix M has identical diagonal entries. Unless specifically mentioned, the inverse temperature $\beta^{-1} = 0.59595$ kcal/mol, corresponding to 300 K. In particular, we take collective variables $\zeta = \xi(x, y) = (x, y)$. In this case, the MFEP becomes a minimum energy path (MEP). Alternatively, an MEP can be considered as an MFEP for which we have an accurate estimate of $F(\zeta)$.

In 3, we show an MEP connecting two local minima through the third local minimum. The MEP has a cusp at the intermediate minimum. The MEPs are computed using the simplified string method with piecewise linear interpolation and equal arc length normalization. The time step $\tau^2 = 0.01$. The iteration is stopped if $d < 0.005$, where

$d = \max_{0 \leq j \leq J} \tau^{-2} |Z_j^{\text{new}} - Z_j|$. From the figure, we can see that the cusp is missing if the number of images ($J + 1 = 10$) is too small. Also, the MEP does not go through the intermediate local minimum as it should, even with many images ($J + 1 = 80$).

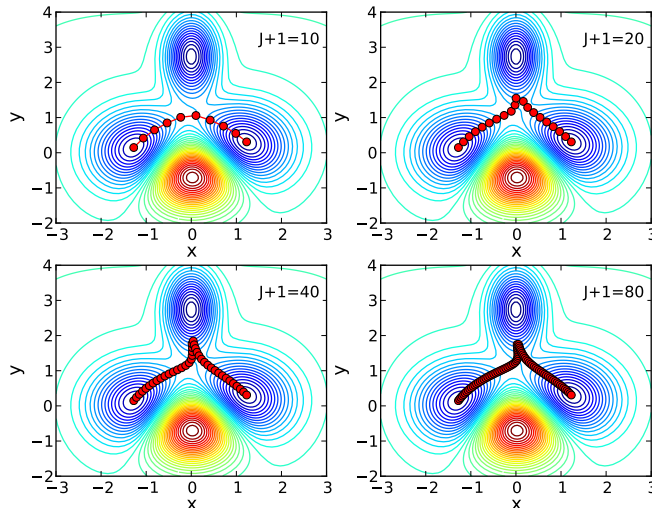


Figure 3: Minimum energy path obtained using the simplified string method. The initial path is the straight line between $(-1, 0)$ and $(1, 0)$. The path is discretized into $J + 1$ images. Four figures are generated using $J + 1 = 10, 20, 40, 80$ images, respectively.

A calculation (not shown here) similar to that for 3 was done for the MFTP. The MFTP is calculated using the semi-implicit simplified string method described in Sec. 4. The MFTP can be resolved using a relatively small set of images, for example, the MFTP calculated by only 10 images ($J = 9$) is almost indistinguishable from the one calculated using 80 images ($J = 79$). The MFTP avoids the cusp problem.

The MFTP generates different paths at different temperature. 4 shows MFTPs at 3 K, 30 K, 300 K, 3000 K, 30000 K, respectively. It is clear that the MFTP is close to the MEP at low temperature (3 K) and is close to a straight line at high temperature (30000 K), which is what we expect.

An FTS method path is expected to be similar to an MFEP for this example.

5.2 Phi, psi for alanine dipeptide in vacuum

For comparison with the MFEP, we study alanine dipeptide at 300 K in vacuum [20]. We compare the MFEP and the MFTP with two dihedral angles ϕ and ψ as collective variables. All simulations were performed using the CHARMM simulation program [4, 5] and the full-atom representation of the molecule in the CHARMM force field [18, 19]. Langevin dynamics with friction coefficient 10.0 ps^{-1} and time step 1.0 fs was used. For the calculation of ∇F

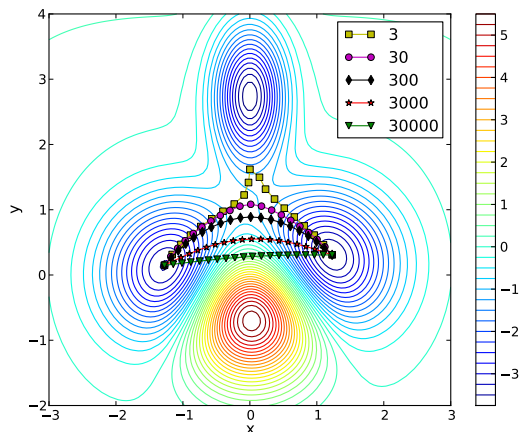


Figure 4: Maximum flux transition path obtained using the semi-implicit simplified string method. Here we used the same initial path and the same stopping criterion for convergence as for 3. The MFTPs are generated using 20 images at 3 K, 30 K, 300 K, 3000 K, 30000 K, respectively (which roughly correspond to $\beta^{-1} = 0.006, 0.06, 0.6, 6, 60$ kcal/mol.) The contour lines are separated by 0.25 kcal/mol.

and D , harmonic potentials as in Eq. (14) were added involving the dihedral angles ϕ and ψ with force constant 1000 kcal/(mol rad²) (corresponding to $\varepsilon = 1^\circ$).

The initial path in collective variable space is a straight line between two points in $\phi - \psi$ space. The path is discretized into $J + 1$ images. The configuration of alanine dipeptide at each image along the initial path is built using the IC module in CHARMM with dihedral angles fixed at the interpolated values. Then follow 1000 steps of minimization and 50,000 steps of heating before the iteration starts. Each iteration of the path involves 50,000 steps of equilibration and 500,000 steps of sampling. The configuration at the final step of sampling in the previous iteration is used as the initial configuration for the equilibration in the next iteration.

We begin by comparing the MFTP and MFEP from $C_{7\text{eq}}$ to $C_{7\text{ax}}$. The MFEP is calculated using the simplified string method with linear interpolation between images and equal arc length normalization. The MFTP is calculated using the semi-implicit simplified string method. In 5, the initial path is the straight line between $(-83.2^\circ, 74.5^\circ)$ and $(70^\circ, -70^\circ)$, which were determined as $C_{7\text{eq}}$ and $C_{7\text{ax}}$ in Ref. [20]. The path is discretized into 20 images. The time step $\tau^2 = 0.16$ in CHARMM time units squared, or $\tau^2 = (19.56 \text{ fs})^2$. The statistical error estimated by block averaging using 32 blocks is $\pm 0.00577^\circ$. The iteration is stopped if $d < 0.02$. (The tolerance value should be chosen properly since the statistical error will eventually dominate the other errors so that d fluctuates about a positive number.) It takes 34 and 31 iterations to converge for the MFTP and MFEP, respectively. The computational cost for two methods is comparable. The path calculated for this problem by the FTS method using the CHARMM force field is given in Figure 5 of Ref. [29].

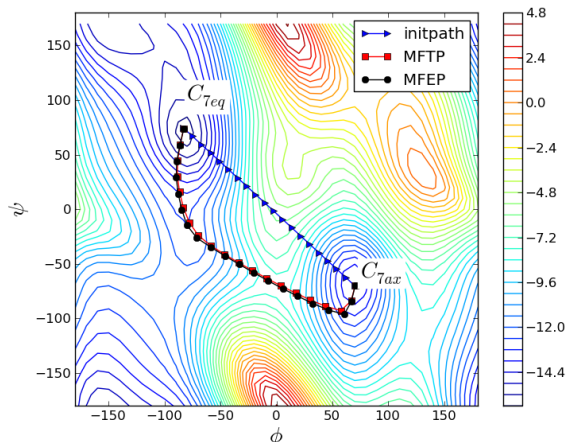


Figure 5: Maximum flux transition path and minimum free energy path from C_{7eq} to C_{7ax} for alanine dipeptide in vacuum at 300 K. Triangles are images of the initial path; rectangles are the images of the maximum flux transition path; and circles are the images of the minimum free energy path. The contours are those for the zero-temperature free energy (adiabatic energy). The contour lines are separated by 0.6 kcal/mol.

Next we compare the MFTP and MFEP from C_{7eq} to C'_{7eq} . In particular, we calculate the transition path $C_{7eq}-C_{7ax}-C'_{7eq}$, in which C_{7ax} serves as an intermediate metastable state. The initial path is taken to be the straight line between $(-80^\circ, 80^\circ)$ and $(190^\circ, -190^\circ)$. 6 shows the MFTP and MFEP generated using 40 images. The time step $\tau^2 = (19.56 \text{ fs})^2$. The iteration is stopped if $d < 0.02$. It takes 35 and 44 iterations for the MFTP and MFEP to converge, respectively. It is evident that the MFTP is more efficient than the MFEP in this case.

5.3 Phi, psi for alanine dipeptide in solution

We also test our method for alanine dipeptide solvated in explicit water. Again, the backbone dihedrals ϕ and ψ are used as collective variables to describe the transition. The initial paths are straight lines connecting two points among $(-77^\circ, 138^\circ)$, $(55^\circ, 48^\circ)$, $(60^\circ, -72^\circ)$, and $(-77^\circ, -39^\circ)$ in (ϕ, ψ) -space.

For preparing the simulation, each starting structure for alanine dipeptide with constrained ϕ and ψ angles is solvated in a $(20 \times 18 \times 15) \text{ \AA}^3$ box with 191 TIP3 [15] water molecules and equilibrated for 50,000 ps. The molecular dynamics are carried out with the CHARMM program under the CHARMM22 force field. Periodic boundary conditions are used and the electrostatic interactions are treated with the particle mesh Ewald method [9]. The system is simulated at a constant pressure of 1.0 atm and a constant temperature 300 K with the algorithm based on Hoover's methods. We use a 1-fs timestep with the SHAKE [30] algorithm to keep all bonds involving hydrogen atoms at fixed lengths.

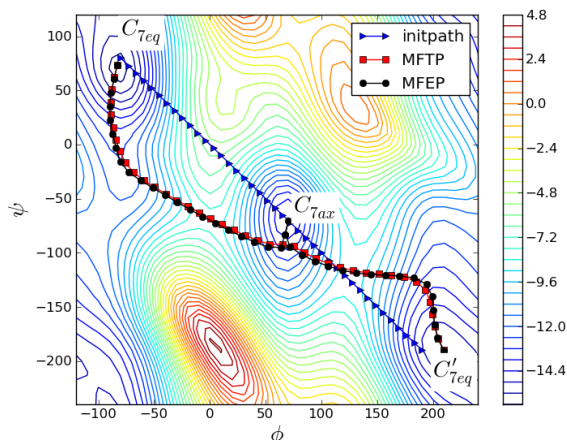


Figure 6: Maximum flux transition path and minimum free energy path for alanine dipeptide from C_{7eq} to C'_{7eq} passing by C_{7ax} in vacuum at 300 K. The figure is generated using 40 images. Triangles are the images for the initial path; rectangles are the images of the maximum flux transition path; and circles are the images of the minimum free energy path. The contours are those for the zero-temperature free energy. The contour lines are separated by 0.6 kcal/mol.

In 7, four MFTPs are calculated using the semi-implicit simplified string method. Each iteration involves 50,000 steps of equilibration and 500,000 steps of sampling. The transition paths are the result of 50 cycles of iteration. The path $C_{7eq}-\alpha_L$ calculated for this problem by the FTP method using the CHARMM force field is given in Figure 12 of Ref. [29]. The MFTP is similar to the FTS method path.

Acknowledgement

This material is based upon work supported by grant R01GM083605 from the National Institute of General Medical Sciences, award A5286056128 from the University of Minnesota, and by a 2007 Purdue Research Foundation Special Incentive Research Grant. We would like to thank Carol Post for the collaboration that nurtured this work. Also, thanks to He Huang for an initial implementation of the string method and an early demonstration of cusps for alanine dipeptide, and to Voichita Dadarlat for 2. Additionally, thanks to Eric Vanden-Eijnden for helpful information about transition path methods and theory, and for suggestions that improved the original manuscript. Finally, thanks to the Center for Biological Physics at Arizona State University and the Institute for Mathematics and Its Applications at the University of Minnesota for providing environments that facilitated this work.

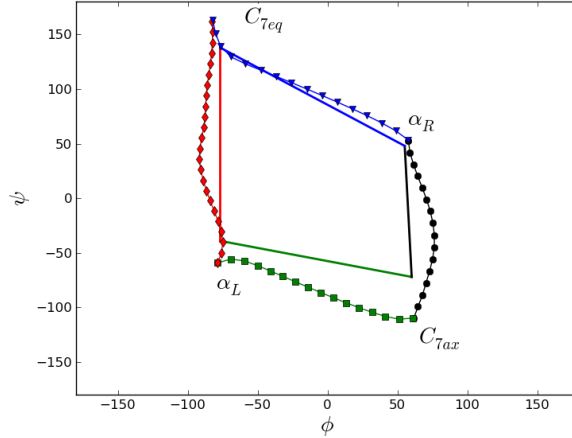


Figure 7: Maximum flux transition paths for alanine dipeptide in solution. The transition paths are calculated by the semi-implicit simplified string method with the nearby straight lines as initial paths.

A Derivation of Brownian dynamics approximation

The quasi-committor is related to a full phase-space committor in Ref. [33] (Sec. 6. 2) q^* defined as follows:

$$q^*(x, p) = \Pr(X(t) \text{ reaches } B \text{ before } A \mid X(0) = x, P(0) = p).$$

Note that $q^*(x, p) = 0$ or 1 , because the dynamical equation is deterministic. By definition, the quasi-committor $\hat{q}(\zeta) = \langle q^*(x, p) \rangle_\zeta$.

It is not difficult to show that $\hat{q}(\xi(x))$ approximates $q^*(x, p)$ in the sense that it minimizes $\langle |q(\xi(x)) - q^*(x, p)|^2 \rangle$ over all $q(\zeta)$. However, this is not useful for determining $\hat{q}(\zeta)$ because $q^*(x, p)$ is too costly to compute. On the other hand, it is possible to find a best approximation to $q^*(x, p)$ in another sense. Because q^* is constant on a trajectory, we have

$$0 = \frac{d}{dt} q^*(X(t), P(t)) = (Lq^*)(X(t), P(t)) \quad \text{where } L = (M^{-1}p) \cdot \nabla_x - U_x \cdot \nabla_p.$$

Consequently, q^* satisfies the stationary Liouville equation

$$Lq^* = 0, \quad q^* = 0 \text{ on } A, \quad q^* = 1 \text{ on } B.$$

Since we do know $Lq^* = 0$, we seek instead an approximation q that minimizes $I(q) = \langle |L(q(\xi(x)) - q^*(x, p))|^2 \rangle$, a standard tactic in numerical analysis. As shown in Sec. III.B of Ref. [20], this simplifies to

$$I(q) = \frac{1}{\beta} \langle |M^{-1/2} \nabla_x q(\xi(x))|^2 \rangle,$$

which is to be as small as possible. A low value for $I(q)$ is attained by having $q(\zeta)$ increase monotonically from the value 0 on A_ξ to the value 1 on B_ξ , which is consistent with the prescription given earlier that $\xi(x)$ be chosen so that the quasi-committor has no local minima or maxima outside of A_ξ and B_ξ .

The functional $I(q)$ can be expressed in terms of collective variables ζ as given by Eq. (2) and shown in in Eq. (15) of Ref. [20].

B Derivation of lasting hitting-point distribution

The proof of Proposition 5 in Ref. [8] (p. 158) analyzes the flux of reactive trajectories. The flux $J(\zeta)$ gives the rate at which such trajectories cross an arbitrary surface Σ that separates collective variable space into two parts, one containing A_ξ and the other containing B_ξ via the integral $\int_\Sigma J(\zeta) \cdot \hat{n}(\zeta) dS_\zeta$ where $\hat{n}(\zeta)$ points to the side containing B_ξ . The proof actually looks not at all crossings but only those occurring within a vanishingly small time interval before the last crossing—see Eq. (50) of Ref. [8]. Therefore, it considers the net flux only in this limiting sense. As the length of the time interval $\tau \rightarrow 0$, the positions of these crossings all converge to the position of the last crossing. So, indeed, one gets the flux of the last hitting point from Proposition 5 of Ref. [8]. The result given in Ref. [8] (Eq. (39)), as well as in Ref. [21] (Eq. (6), Eq. (A12)), and Ref. [33] (Eq. (62)), is that the last hitting-point flux for reactive trajectories is $J(\zeta) = \rho_\xi(\zeta) D(\zeta) \nabla q(\zeta)$. (Proposition 4 of Ref. [8] does not apply to the infinitely damped case of Langevin dynamics.) That the expression for $J(\zeta)$ also gives the net flux of reactive trajectories is Eq. (32) of Ref. [33]. Also, the formula for $j(\zeta)$ in Sec. 3.2 agrees in the special case $D = I$ with that for the *first* hitting point distribution given in Ref. [37] (Appendix B). Last and first are the same for reversible dynamics like Brownian dynamics. Finally, there is an example in Metzner, Schütte, and Vanden-Eijnden (2006) section III.C, where it is suggested to use $\hat{n} \cdot J$.

C Derivation of the maximum flux condition

We have from (1) and (6) that the normal flux is

$$j(\zeta) = \text{const}_\xi e^{-\beta F(\zeta)} \bar{q}_s(\sigma(\zeta)) \nabla \sigma(\zeta)^\top D(\zeta) \nabla \sigma(\zeta) / |\nabla \sigma(\zeta)| \quad (15)$$

where $\sigma(\zeta)$ is defined implicitly by $q(\zeta) = \bar{q}(\sigma(\zeta))$. And for each point $Z(s)$ on the desired path, the condition to be satisfied (7) is $\nabla j(Z(s)) \parallel n(s)$. We also approximate $D(\zeta)$ by $\bar{D}(\sigma(\zeta))$ where $\bar{D}(s) \stackrel{\text{def}}{=} D(Z(s))$. Furthermore, the assumption (8) that isocommittors are planar implies

$$n(\sigma(\zeta)) \cdot (\zeta - Z(\sigma(\zeta))) = 0. \quad (16)$$

Differentiating Eq. (16) w.r.t. ζ , we get

$$(n_s(\sigma) \cdot (\zeta - Z(\sigma)) - n(\sigma) \cdot Z_s(\sigma)) \nabla \sigma + n(\sigma) = 0,$$

where the argument ζ of σ has been omitted, whence

$$\nabla\sigma = (n(\sigma) \cdot Z_s(\sigma) - n_s(\sigma) \cdot (\zeta - Z(\sigma)))^{-1}n(\sigma). \quad (17)$$

Substituting Eq. (17) into Eq. (15) and replacing $D(\zeta)$ by $\bar{D}(\sigma(\zeta))$, the normal flux becomes

$$j(\zeta) = \varphi(\sigma(\zeta), \zeta),$$

where

$$\varphi(s, \zeta) = \text{const} \xi e^{-\beta F(\zeta)} \bar{q}_s(s) (n(s) \cdot Z_s(s) - n_s(s) \cdot (\zeta - Z(s)))^{-1} n(s)^\top \bar{D}(s) n(s) / |n(s)|.$$

Note that

$$\frac{\nabla_\zeta \varphi}{\varphi} = -\beta \nabla F + \frac{n_s}{n \cdot Z_s - n_s \cdot (\zeta - Z)},$$

and

$$\left. \frac{\nabla_\zeta \varphi}{\varphi} \right|_{\zeta=Z} = -\beta \nabla F(Z) + \frac{n_s}{n^\top Z_s}.$$

Thus, we have

$$\frac{\nabla j}{j} = \frac{(\nabla_\zeta \varphi)(\sigma(\zeta), \zeta)}{\varphi(\sigma(\zeta), \zeta)} + \frac{\varphi_s(\sigma(\zeta), \zeta)}{\varphi(\sigma(\zeta), \zeta)} \nabla \sigma(\zeta),$$

and

$$\left. \frac{\nabla j}{j} \right|_{\zeta=Z} = -\beta \nabla F(Z) + \frac{n_s}{n^\top Z_s} + \frac{\varphi_s(s, Z) n}{\varphi(s, Z) n(s)^\top Z_s(s)}.$$

Hence, the condition is that

$$-\beta \nabla F(Z) + \frac{n_s}{n^\top Z_s} \parallel n.$$

References

- [1] M. Berkowitz, J. D. Morgan, J. A. McCammon, and S. H. Northrup. Diffusion-controlled reactions: A variational formula for the optimum reaction coordinate. *J. Chem. Phys.*, 79:5563–5565, 1983.
- [2] P. G. Bolhuis, D. Chandler, C. Dellago, and P. L. Geissler. Transition path sampling: Throwing ropes over rough mountain passes, in the dark. *Annu. Rev. Phys. Chem.*, 53:291–318, 2002.
- [3] P. G. Bolhuis, C. Dellago, and D. Chandler. Reaction coordinates of biomolecular isomerization. *PNAS*, 97:5877–5882, 2000.
- [4] B. R. Brooks, C. L. Brooks III, A. D. MacKerell Jr., L. Nilsson, R. J. Petrella, B. Roux, Y. Won, G. Archontis, C. Bartels, S. Boresch, A. Caffisch, L. Caves, Q. Cui, A. R. Dinner, M. Feig, S. Fischer, J. Gao, M. Hodoscek, W. Im, K. Kuczera, T. Lazaridis, J. Ma, V. Ovchinnikov, E. Paci, R. W. Pastor, C. B. Post, J. Z. Pu, M. Schaefer, B. Tidor, R. M. Venable, H. L. Woodcock, X. Wu, W. Yang, D. M. York, and M. Karplus. CHARMM: The biomolecular simulation program. *J. Comput. Chem.*, 30:1545–1614, 2009.

- [5] B. R. Brooks, R. E. Bruccoleri, B. D. Olafson, D. J. States, S. Swaminathan, and M. Karplus. CHARMM: A program for macromolecular energy, minimization, and dynamics calculations. *J. Comput. Chem.*, 4:187–217, 1983.
- [6] W. E, W. Ren, and E. Vanden-Eijnden. Simplified and improved string method for computing the minimum energy paths in barrier-crossing events. *J. Chem. Phys.*, 126:164103, 2007.
- [7] W. E and E. Vanden-Eijnden. Metastability, conformation dynamics, and transition pathways in complex systems. In S. Attinger, editor, *Multiscale Modelling And Simulation*, pages 35–68. Springer Verlag, 2004.
- [8] W. E and E. Vanden-Eijnden. Towards a theory of transition paths. *J. Stat. Phys.*, 123:503–523, 2006.
- [9] U. Essmann, L. Perera, M. L. Berkowitz, T. Darden, H. Lee, and L. Pederson. A smooth particle mesh Ewald method. *J. Chem. Phys.*, 103:8577–8593, 1995.
- [10] D. Frenkel and B. Smit. *Understanding Molecular Simulation: From Algorithms to Applications*. Academic Press, 2002.
- [11] W. Gan, S. Yang, and B. Roux. Atomistic view of the conformational activation of Src kinase using the string method with swarms-of-trajectories. *Biophys. J.*, 97:L8–L10, 2009.
- [12] H. Huang, E. Ozkirimli, and C. B. Post. Comparison of three perturbation molecular dynamics methods for modeling conformational transitions. *J. Chem. Theory Comput.*, 5:1304–1314, 2009.
- [13] S. Huo and J. E. Straub. The MaxFlux algorithm for calculating variationally optimized reaction paths for conformational transitions in many body systems at finite temperature. *J. Chem. Phys.*, 107:5000–5006, 1997.
- [14] H. Jónsson, G. Mills, and K. W. Jacobsen. Nudged elastic band method for finding minimum energy paths of transitions. In B. J. Berne, G. Ciccotti, and D. F. Coker, editors, *Classical and Quantum Dynamics in Condensed Phase Simulations*, page 385. World Scientific, Singapore, 1998.
- [15] W. L. Jorgensen, J. Chandrasekhar, J. D. Madura, R. W. Impey, and M. L. Klein. Comparison of simple potential functions for simulating liquid water. *J. Chem. Phys.*, 79:926–935, 1983.
- [16] M. Lei, M. I. Zavodszky, L. A. Kuhn, and M. F. Thorpe. Sampling protein conformations and pathways. *J. Comput. Chem.*, 25:1133–1148, 2004.
- [17] A. Ma and A. R. Dinner. Automatic method for identifying reaction coordinates in complex systems. *J. Phys. Chem. B*, 109:6769–6779, 2005.

- [18] A. D. MacKerell Jr., D. Bashford, M. Bellott, R. L. Dunbrack Jr., J. D. Evanseck, M. J. Field, S. Fischer, J. Gao, H. Guo, S. Ha, D. Joseph-McCarthy, L. Kuchnir, K. Kuczera, F. T. K. Lau, C. Mattos, S. Michnick, T. Ngo, D. T. Nguyen, B. Prodhom, W. E. Reiher, III, B. Roux, M. Schlenkrich, J. C. Smith, R. Stote, J. Straub, M. Watanabe, J. Wiórkiewicz-Kuczera, D. Yin, and M. Karplus. All-atom empirical potential for molecular modeling and dynamics studies of proteins. *J. Phys. Chem. B*, 102:3586–3616, 1998.
- [19] A. D. Mackerell Jr., M. Feig, and C. L. Brooks III. Extending the treatment of backbone energetics in protein force fields: Limitations of gas-phase quantum mechanics in reproducing protein conformational distributions in molecular dynamics simulations. *J. Comput. Chem.*, 25:1400–1415, 2004.
- [20] L. Maragliano, A. Fischer, E. Vanden-Eijnden, and G. Ciccotti. String method in collective variables: Minimum free energy paths and isocommittor surfaces. *J. Chem. Phys.*, 125:024106, 2006.
- [21] P. Metzner, C. Schütte, and E. Vanden-Eijnden. Illustration of transition path theory on a collection of simple examples. *J. Chem. Phys.*, 125:084110, 2006.
- [22] R. Olender and R. Elber. Calculation of classical trajectories with a very large time step: Formalism and numerical examples. *J. Chem. Phys.*, 105:9299–9315, 1996.
- [23] L. Onsager. Initial recombination of ions. *Phys. Rev.*, 54:554–557, 1938.
- [24] E. Ozkirimli and C. B. Post. Src kinase activation: A switched electrostatic network. *Protein Sci.*, 15:1051–1062, 2006.
- [25] E. Ozkirimli, S. S. Yadav, T. W. Miller, and C. B. Post. An electrostatic network and long-range regulation of Src kinases. *Protein Sci.*, 17:1871–1880, 2008.
- [26] A. C. Pan, D. Sezer, and B. Roux. Finding transition pathways using the string method with swarms of trajectories. *J. Phys. Chem. B*, 112:3432–3440, 2008.
- [27] S. Park, M. K. Sener, D. Lu, and K. Schulten. Reaction paths based on mean first-passage times. *J. Chem. Phys.*, 119:1313–1319, 2003.
- [28] J. C. Phillips, R. Braun, W. Wang, J. Gumbart, E. Tajkhorshid, E. Villa, C. Chipot, R. D. Skeel, L. Kalé, and K. Schulten. Scalable molecular dynamics with NAMD. *J. Comput. Chem.*, 26:1781–1802, 2005.
- [29] W. Ren, E. Vanden-Eijnden, P. Maragakis, and W. E. Transition pathways in complex systems: Application of the finite-temperature string method to the alanine dipeptide. *J. Chem. Phys.*, 123:134109, 2005.

- [30] J.-P. Ryckaert, G. Ciccotti, and H. J. C. Berendsen. Numerical integration of the cartesian equations of motion of a system with constraints: molecular dynamics of n-alkanes. *J. Comput. Phys.*, 23:327 – 341, 1977.
- [31] J. Schlitter, M. Engels, and P. Krüger. Targeted molecular dynamics: A new approach for searching pathways of conformational transitions. *J. Mol. Graphics*, 12:84–89, 1994.
- [32] N. Singhal and V. S. Pande. Error analysis and efficient sampling in Markovian state models for molecular dynamics. *J. Chem. Phys.*, 123:204909, 2005.
- [33] E. Vanden-Eijnden. Transition path theory. In K. Binder, G. Ciccotti, and M. Ferrario, editors, *Computer Simulations in Condensed Matter: From Materials to Chemical Biology, Volume 2*, Lecture Notes in Physics, pages 453–493. Springer, Berlin, 2006.
- [34] E. Vanden-Eijnden. Theoretical equivalence between original string and swarm string in the short lag limit. Unpublished work, 2008.
- [35] E. Vanden-Eijnden and M. Heymann. The geometric minimum action method for computing minimum energy paths. *J. Chem. Phys.*, 128:061103, 2008.
- [36] E. Vanden-Eijnden and M. Venturoli. Revisiting the finite temperature string method for the calculation of reaction tubes and free energies. *J. Chem. Phys.*, 130:194103, 2009.
- [37] E. Vanden-Eijnden, M. Venturoli, G. Ciccotti, and R. Elber. On the assumptions underlying milestoning. *J. Chem. Phys.*, 129:174102, 2008.
- [38] S. Yang, N. K. Banavali, and B. Roux. Mapping the conformational transition in Src activation by cumulating the information from multiple molecular dynamics trajectories. *PNAS*, 106:3776–3781, 2009.
- [39] J. Zhang, P. L. Yang, and N. S. Gray. Targeting cancer with small molecule kinase inhibitors. *Nat. Rev. Cancer*, 9:28–39, 2009.
- [40] R. Zhao. Mftp code, 2009. URL <http://bionum.cs.purdue.edu/mftp>.

Captions

Figure 1: A schematic illustration of a poor choice of collective variables. The horizontal axis is collective variables, and the vertical axis is unrepresented degrees of freedom. The collective variables fail to indicate the progress of the reaction.

Figure 2: Shading indicates contours of free energy, thin curves denote isocommitters, ellipses enclose concentrations of crossing points from reactive trajectories, and the thick curve is the center.

Figure 3: Minimum energy path obtained using the simplified string method. The initial path is the straight line between $(-1, 0)$ and $(1, 0)$. The path is discretized into $J + 1$ images. Four figures are generated using $J + 1 = 10, 20, 40, 80$ images, respectively.

Figure 4: Maximum flux transition path obtained using the semi-implicit simplified string method. Here we used the same initial path and the same stopping criterion for convergence as for 3. The MFTPs are generated using 20 images at 3 K, 30 K, 300 K, 3000 K, 30000 K, respectively (which roughly correspond to $\beta^{-1} = 0.006, 0.06, 0.6, 6, 60$ kcal/mol.) The contour lines are separated by 0.25 kcal/mol.

Figure 5: Maximum flux transition path and minimum free energy path from $C_{7_{\text{eq}}}$ to $C_{7_{\text{ax}}}$ for alanine dipeptide in vacuum at 300 K. Triangles are images of the initial path; rectangles are the images of the maximum flux transition path; and circles are the images of the minimum free energy path. The contours are those for the zero-temperature free energy (adiabatic energy). The contour lines are separated by 0.6 kcal/mol.

Figure 6: Maximum flux transition path and minimum free energy path for alanine dipeptide from $C_{7_{\text{eq}}}$ to $C'_{7_{\text{eq}}}$ passing by $C_{7_{\text{ax}}}$ in vacuum at 300 K. The figure is generated using 40 images. Triangles are the images for the initial path; rectangles are the images of the maximum flux transition path; and circles are the images of the minimum free energy path. The contours are those for the zero-temperature free energy. The contour lines are separated by 0.6 kcal/mol.

Figure 7: Maximum flux transition paths for alanine dipeptide in solution. The transition paths are calculated by the semi-implicit simplified string method with the nearby straight lines as initial paths.